Julia Sammer, BSc

Sensitivity of Cut-Off Low Detection and Tracking Methods in the Northern Hemisphere

Master Thesis

to achieve the university degree of

Master of Science

Master's degree programme: Space Science and Earth From Space

submitted to

Graz University of Technology

Supervisor

Assoz. Prof. Dr. Douglas Maraun

Wegener Center for Climate and Global Change

Regional Climate Research Group

Karl-Franzens-University of Graz

Graz, February 2021

Affidavit

I declare that I have authored this thesis independently, that I have not used other than the declared sources/resources, and that I have explicitly indicated all material which has been quoted either literally or by content from the sources used. The text document uploaded to TUGRAZonline is identical to the present master's thesis.

_____   _____
            Date   Signature

Abstract

Atmospheric processes are often described in terms of empirical conceptual models, which aim to reproduce previously observed structures and characteristics. For the cut-off low, an upper-tropospheric low pressure system often associated with extreme precipitation events in the mid-latitudes, the scientific consensus on the structure is low, leading to inconsistencies among previous cut-off low climatologies.

Motivated by these inconsistencies, the current thesis analyses previous cut-off low detection and tracking methods used in the Northern Hemisphere, as well as implements a new method based on a cyclone detection algorithm. This new approach neglects uncertain assumptions of cut-off low structure, especially the vertical position of the cold core, and focuses on robust characteristics, namely the low pressure at the center and the cyclonic circulation around the center. Cut-off lows have been detected and tracked on ERA5 reanalysis data (geopotential height and relative vorticity at 300 hPa, respectively) for the period 1979 to 2019. Additional filters based on

the direction of meridional and zonal winds at 300 hPa have been applied to ensure a cyclonic circulation.

Compared to previous studies, the method implemented in this thesis detects notably higher frequencies in cut-off low occurrence, with more events being detected on the geopotential height field than the relative vorticity field. Tracking on both fields yields a positive trend in cut-off low occurrence, though different magnitudes have been detected. Furthermore, tracking on the geopotential height agrees with the pattern of seasonality found in previous studies, while for the relative vorticity field certain regions experience a decrease in summer events. It has been shown that the presented method poses an alternative to previous detection methods, though further tuning of the configuration parameters has to be performed.

Zusammenfassung

Die Beschreibung von Prozessen innerhalb der Atmosphäre erfolgt oft über empirisch-konzeptionelle Modelle, welche auf beobachteten Charakteristiken beruhen. Im Falle eines Cut-Off Lows, einem mit Extremniederschlägen assoziierten Tiefdruckgebietes in der oberen Troposphärenschicht, ist der wissenschaftliche Konsensus bezüglich dominanter Eigenschaften innerhalb des Prozesses gering, was sich in Widersprüchen bisheriger Forschungsergebnisse wiederspiegelt.

Angetrieben von diesen Widersprüchen ist das Ziel dieser Diplomarbeit die Analyse von bisher in der Nordhemisphäre verwendeten Detektionsverfahren, und die Implementierung eines neuen Verfahrens beruhend auf einem Zyklon-Detektionsalgorithmus. Dabei wird auf umstrittene Annahmen, wie beispielsweise die Höhe des Kältezentrums, verzichtet. Stattdessen beruht die Detektion auf robusten Charakteristiken eines Cut-Off Lows, nämlich die Existenz eines Druckminimums im Zentrum, und einer zyklonalen Rotation um das Zentrum. Cut-Off Lows sind demnach in ERA5 Reanalysedaten für den Zeitraum 1979-2019 detektiert worden, sowohl in

geopotentiellen Höhedaten, als auch im Feld der relativen Vorticity auf 300 hPa. Um die zyklonale Rotation zu gewährleisten wurden zusätzliche Filter basierend auf merdionalen und zonalen Windrichtungen in einer Höhe von 300 hPa angewendet.

Verglichen mit bisherigen Studien werden mit der hier vorgestellten Methode mehr Cut-Off Lows detektiert. Die Detektion auf dem Feld der geopotentiellen Höhe liefert zudem mehr Events, als die Detektion auf dem Feld der relativen Vorticity. Die Cut-Off Lows aus beiden Feldern zeigen einen positiven Trend bezüglich der jährlichen Events für den betrachteten Zeitraum, wobei sie sich in der Stärke des Trends unterscheiden. Bezüglich der Saisonalität zeigt die Detektion auf dem Feld der relativen Vorticity ein Sommer-Minimum, während die auf der geopotentiellen Höhe detektierten Events mit bisherigen Studien übereinstimmen. Die vorgestellte Methode eignet sich grundsätzlich dazu Cut-Off Lows zu detektieren, jedoch sind weitere Tests notwendig um die bestmögliche Konfiguration des Algorithmus zu bestimmen.

Contents

Acronyms

DJF Winter (December, January, February)

gpm Geopotential Meters

JJA Summer (June, July, August)

MAM Spring (March, April, May)

NH Northern Hemisphere

NRMSE Normalized Root Mean Square Error

PV Potential Vorticity

PVU Potential Vorticity Unit

RMSE Root Mean Square Error

RWB Rossby Wave Breaking

SON Autumn (September, October, November)

TFP Thermal Front Parameter

1. Introduction

In recent years, the demand for actionable information on climate change has grown. As the earth's energy budget is changing under anthropogenic greenhouse gas emissions, policy-makers and stakeholders are confronted with dramatic future scenarios. To foster the construction of effective adaptation strategies, scientists and modelling groups on the whole planet have focused on simulating the climate system via climate models, and creating projections of the future climate under various emission scenarios.

In order to assess the credibility of such climate models, their skill in simulating climate processes at varying scales is evaluated. These process-based evaluations require fundamental knowledge of the processes involved, and often rely on conceptual models and frameworks, which themselves inherit assumptions and uncertainties. An example of such a process is the cut-off low, which is an upper-tropospheric low pressure system occurring in the mid-latitudes, and often associated with extreme precipitation events (e.g. Porcù et al. (2007), Awan and Formayer (2017)). The prediction of cut-off low associated precipitation poses a considerable challenge, due to the high

dependency on moisture availability and orography (Nieto et al. (2008)). Studies disagree on key metrics characterizing cut-off lows, such as historical trend in cut-off low occurrence or absolute number of annual events (Muñoz et al. (2020)). Furthermore, studies in the Northern and Southern Hemisphere disagree on where and when precipitation falls within a cut-off low. Two possible explanations for varying dynamics among Hemispheres have been given by Pinheiro et al. (2020), which are either regional differences in the onset and lifetime of cut-off lows and the associated precipitation, or a strong sensitivity to the detection scheme used. Especially detection schemes based on assumptions of a cold core at high vertical levels (200 hPa) fail to detect cut-off lows in certain regions (Guo et al. (2021)), yet most long-term Northern Hemisphere cut-off low climatologies are based on imposing a cold-core criterion on geopotential height minima at 200 hPa (e.g. Nieto et al. (2005), Muñoz et al. (2020)).

In order to assess the sensitivity of detection scheme used to detect cut-off lows, Pinheiro et al. (2019) implemented an algorithm based on the cyclone detection tool TRACK (Hodges (1994, 1995, 1999)), and detected relative vorticity and geopotential minima in the Southern Hemisphere at 300 hPa respectively[1]. To ensure the detection of closed cyclonic circulations, three additional filters based on wind directions at different offset radial distances around the low pressure/vorticity center have been implemented. Furthermore, by imposing additional temperature and potential vorticity

---

[1]Note that in the Northern Hemisphere cyclonic circulation is associated with maxima in the relative vorticity field, instead of minima.

criteria, it has been shown that the cut-off low number and seasonality are strongly affected by the choice of method.

Climatologies in the Northern Hemisphere are usually based on the conceptual cut-off low model by Nieto et al. (2005), which assumes a cold core at the cut-off low center, and a thickness ridge as well as a baroclinic zone ahead of the low. The model itself is based on case studies of European and North-American cut-off lows, yet it is unclear how well the model captures cut-off low structure in general, and if the derived algorithm applies well to gridded data. Therefore the question naturally arises if the sensitivity of cut-off low detection previously found in the Southern Hemisphere also applies to Northern Hemisphere cut-off lows, and furthermore if previous Northern Hemisphere cut-off low climatologies are biased as a result of a flawed detection scheme.

Motivated by these uncertainties, the current thesis aims to strengthen the understanding of Northern Hemisphere cut-off lows by considering the following question:

1. What detection schemes exist to detect cut-off lows, and how to they differ?
2. Does the choice of method to detect cut-off lows introduce an additional source of uncertainty in the Northern Hemisphere? In other words, how robust are previously derived cut-off low metrics, such as number of events, seasonality, intensity, persistance or trends?

3. Is the recent implementation of the cyclone detection tool TRACK by Pinheiro et al. (2019) for Southern Hemisphere cut-off lows suitable to detect cut-off lows in the Northern Hemisphere? Does the method produce similar results among hemispheres?

4. And lastly, is there a difference in cut-off low metrics among the two fields of detection, namely geopotential height and relative vorticity?

While question 1 will be answered by reviewing previous research, question 2, 3 and 4, aiming to answer open question in the field, will be considered by implementing TRACK to detect cut-off low systems in the Northern Hemisphere. The cut-off low definition used is the one proposed by Palmén (1949), after which a cut-off low is a cyclonic circulating system in the upper troposphere detached from the westerlies. This definition is independent of the vertical location of the cold core, and therefore less vulnerable to uncertain assumptions of cut-off low structure. Comparing cut-off lows detected with TRACK to systems detected with the conceptual model allows to evaluate the sensitivity to the choice of method. Furthermore, comparing the results with the ones derived from Pinheiro et al. (2019) for Southern Hemisphere cut-off lows helps to understand the strength and weaknesses of TRACK.

The thesis is structured as follows: section 2 gives an overview of cut-off low characteristics, reviews two common detection schemes and presents previous research on the topic. Section 3 describes the cyclone detection algorithm TRACK, and how it has been applied in order to detect cut-

off lows on geopotential height and relative vorticity fields at 300 hPa respectively, with additional filtering for a cut-off circulation (using zonal and meridional wind at 300 hPa). The results are presented and further discussed in section 4, and the conclusion is drawn in section 5.

2. Background

This chapter presents a brief review of cut-off low characteristics, such as their horizontal and vertical structure, as well as their temporal evolution. Furthermore, two detection schemes are presented: the first one is based on the conceptual model of cut-off lows by Nieto et al. (2005), which detects geopotential minima on a pressure surface, whereas the second one is based on a contour searching algorithm on an isentropic surface, first introduced by Hoskins et al. (1985). Finally, previous cut-off low climatologies are presented, and discussed in terms of consensus and contradictions.

2.1. Structure of Cut-Off Lows

2.1.1. Definition and Evolution

Cut-off lows are middle- and upper tropospheric low pressure systems, forming in the baroclinic westerlies on the equatorward side of the polar

and subtropical jetstream. They develop from bulk meridional exchange of air masses, namely through the deepening of pre-existing cold troughs (Palmén (1949), Palmén and Newton (1969)). As the cold-air mass within the trough moves equatorward, it is exposed to strong subsidence, which leads to an intensification of the vorticity by vertical stretching of the trough, as well as horizontal convergence upstream. The subsidence is stronger at the center of the trough than it is equatorward, isolating the air mass from its source region at high levels (Crocker et al. (1947)). The systems are described as quasi-stationary, and their irregular trajectories remain a challenge for forecasting systems. Their displacement mainly depends on the strength and direction of the steering current. Only when the steering current is weak does the motion of the system depend on the motion within the cut-off low itself (Hsieh (1949)).

The life cycle of a cut-off low can be separated into four stages, as depicted in Fig. 2.1: the upper level trough, the tear-off, the cut-off and the final stage (Nieto et al. (2005)). In the upper level trough stage the temperature wave is located behind the geopotential wave, with cold advection within the trough, and warm advection on the ridge of the geopotential wave. In this stage the amplitude of the wave increases, while the wavelength decreases (Nieto et al. (2005)).

The tear-off stage is characterized by the formation of an inverse omega shape of the isohypses. The trough deepens further, and it begins to detach from the main meridional and zonal stream. Once the upper trough is completely detached, the cut-off stage is reached. On isobaric surfaces the

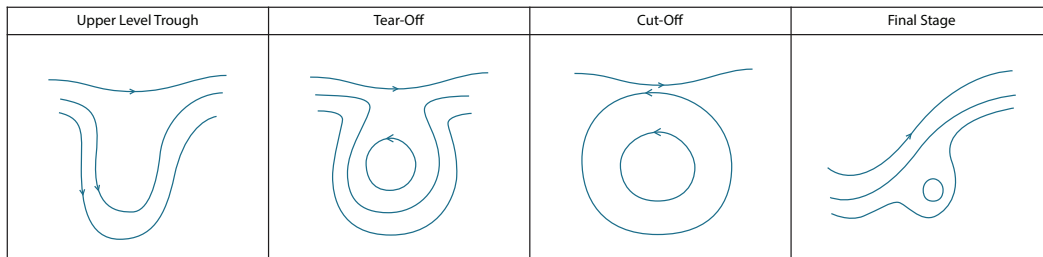| Upper Level Trough	Tear-Off	Cut-Off	Final Stage

Figure 2.1.: Typical life stages of a cut-off low in terms of geopotential height contours at 200 hPa, based on Fig. 1 in Nieto et al. (2005).

cut-off low now shows as closed geopotential contours (Price and Vaughan (1992)). Eventually the cut-off low reaches its final stage, where it either dissolves by convection, or merges with a large upper trough or newly formed cut-off low.

The formation of cut-off lows can be accompanied by the formation of an anticyclonic cut-off high. The process of formation is similar, with warm air advecting polewards and detaching from the source region. In terms of diabatic modifications, the two systems differ. Within a cut-off low deep convection is enhanced, while for the blocking anticyclone convection is suppressed. The cut-off high decays either by radiative cooling, or by re-merging into its source region (Hoskins et al. (1985)).

Hoskins et al. (1985) provided the first description of cut-off lows in terms of isolated regions of high Potential Vorticity (PV) on isentropic surfaces. PV values are usually low in the troposphere, and increase rapidly in the stratosphere, associated with changes in static stability. As PV is conserved

under the assumption of adiabatic motion and the absence of friction, cut-off lows can be traced as high PV anomalies. Cut-off low genesis is then explained in terms of Rossby Wave Breaking (RWB) events, caused by the equatorward advection of stratospheric air into the troposphere along isentropic surfaces (Hoskins et al. (1985), Ndarana and Waugh (2010)).

2.1.2. Vertical Structure

The strongest intensities of cut-off lows are found in the upper-troposphere, close to the tropopause. The vortex weakens in intensity in lower altitudes and often disappears completely at surface layers. There are, however, cut-off lows with an associated anticyclonic circulation at the surface, generally developing towards the final stage of the cut-off low (Hoskins et al. (1985), Porcù et al. (2007)). The anticyclonic vortex at surface layers can gradually change into a cyclonic one, if spreading of the vortex occurs downwards (Palmén (1949)).

Due to their high-latitude origin, the air within the cut-off low is anomalously colder than the surrounding air, and the tropopause is especially low. This gives rise to the potential of tropopause folding around the flank of a cut-off low, and the irreversible intrusion of stratospheric air into the troposphere, changing the composition of the tropospheric air (for example by increasing the ozone concentration, Price and Vaughan (1993), Ravetta and Ancellet (2000)). The stratospheric air located on top of a cut-off

low is anomalously warm, decreasing its intensity with height above the tropopause (Palmén (1949), Pinheiro et al. (2020)).

2.1.3. Circulation and Associated Precipitation

Cut-off lows have been linked to major extreme precipitation and flooding events, for example over Europe (Emanuel (2005), Llasat et al. (2007), Awan and Formayer (2017)), South Africa (Singleton and Reason (2007)), eastern Asia (Zhao and Sun (2007)), North America (Shepherd et al. (2011)) and South America (Bozkurt et al. (2016)). Their contribution to overall rainfall varies with region. As stated by Abatzoglou (2016) about one-third of growing-season (spring-summer) precipitation across the semiarid northern Great Plains (United States) is attributable to cut-off lows, making them indispensable for dryland agriculture in the region and highlighting their importance in ensuring food security.

Persistence and associated precipitation of a cut-off low strongly depend on thermal and orographic surface conditions. Cut-off lows are regions of high static stability (Hoskins et al. (1985), Llasat et al. (2007)). Because of the necessity to maintain balance between the thermal field and the wind fields, the cut-off low itself acts as a de-stabilizer of the air below, giving rise to the development of deep convective systems, assuming a sufficient supply of moisture (Hoskins et al. (1985)). If moisture supply is insufficient, for example over continental areas during winter months, convection is limited, and cut-off lows can persist much longer.

According to Hoskins et al. (1985), cut-off lows last about two days until they dissolve due to diabatic heating. While modern climatologies confirm that a large part of events do not last more than two days, there is still a considerable number of events lasting longer, some more than ten days, and according to Price and Vaughan (1992) some systems last up to three weeks. An explanation for an increased lifetime is given in Price and Vaughan (1993), which is the possibility of re-intensification of cut-off lows by injecting high PV air into the cyclonic vortex, and therefore prolonging its lifetime. In their case study on stratosphere-troposphere exchange of mass within cut-off lows, the authors found that re-intensification typically occurs every three to six days.

Llasat et al. (2007) states that in order for a cut-off low to produce high rainfall it is necessary, though not sufficient, for it to extend down to lower levels. This is supported by Porcù et al. (2007), who found that deep cut-off lows in the Mediterranean produce the highest amount of rainfall, as opposed to shallow cut-off lows, which often do not produce any precipitation at all.

Cut-off lows show asymmetric patterns in cloud cover and precipitation occurrence. Early studies, such as Palmén and Newton (1969), state that deep convection occurs on the eastern edge of the vortex, while clear weather is present west of the cut-off low. In contrast, studies of the cloud cover over Europe suggest that deep convective clouds can also be present west of the cut-off low (Delgado et al. (2007), Nieto et al. (2008)).

Differences in literature can also be found when studying precipitation rates with respect to the life stage of a cut-off low. Studies of European cut-off low systems found the highest rates of precipitation in earlier life stages (Delgado et al. (2007), Nieto et al. (2008)), while studies for South American cut-off lows found that precipitation peaks at later life stages (Satyamurty and Seluchi (2007), Pinheiro et al. (2020)). If these discrepancies result from regional differences or the usage of different definitions of cut-off lows are yet to be investigated.

2.2. Detection of Cut-Off Lows

2.2.1. Detection on Geopotential Height Maps

Bell and Bosart (1989) presented one of the first multidecadal climatologies of cut-off lows, based on the detection of geopotential height minima at 500 hPa. Nieto et al. (2005) developed the approach further, and defined a conceptual model. For that, the authors introduced additional conditions to be met in order for an upper level low to be considered a cut-off low. Two additional fields are used, zonal wind and temperature, and the systems are identified by means of three consecutive steps, which are

1) The detection of geopotential height minima and cut-off circulation at 200 hPa.

2) The identification of a thickness ridge in front of the low, and a trough or a distinct minimum behind or at the center of the low.

3) The computation of the Thermal Front Parameter (TFP) with higher values located east of the cut-off low, representing a baroclinic zone in the frontal region.

The conditions are imposed as gridpoint-wise manipulation, meaning each gridpoint is evaluated separately, and if all three conditions apply, the point is tagged as a cut-off low.

For condition 1) to be fulfilled, six out of the eight surrounding gridpoints have to have higher geopotential height values by at least 10 Geopotential Meters (gpm). Also, there has to be a change in the zonal wind direction in any of the two gridpoints located northwards.

To assess whether or not condition 2) holds true, data on two pressure levels are being used to calculate the thickness of the atmosphere between two pressure surfaces (in the original study the chosen pressure levels are 200 and 300 hPa). The computed values for the equivalent thickness must be higher eastward of the gridpoint than at the gridpoint itself.

The third condition makes use of the characteristic of a baroclinic zone being situated in front of a cut-off low. A measure to locate fronts is the TFP, which is defined as the change of the temperature gradient ∇T in the direction of the temperature gradient. It is calculated via

$$TFP = -\nabla|\nabla T| \cdot \frac{\nabla T}{|\nabla T|} \tag{2.1}$$

13

Finally, in order for the third condition to be true, the TFP-value east of the gridpoint has to be higher than the TFP-value at the central point.

Once the gridpoints associated with cut-off lows are determined, further rules are applied. Several gridpoints are attributed to the same cut-off low event if they are adjacent, and the northernmost and westernmost gridpoint is being used as the representative position of the cut-off low in spatial analysis. To connect cut-off lows over consecutive frames in time, gridpoints are being considered to belong to the same event if a contiguous gridpoint is found in the next frame.

Muñoz et al. (2020) applied an adapted version of the conceptual model. Here, a change in zonal wind direction must be present in one of the four (instead of two) gridpoints located poleward.

Studies on Southern Hemisphere cut-off lows typically use the modified detection approach by Reboita et al. (2010). According to the authors, visual inspections of cut-off lows in the Southern Hemisphere show a pronounced westward tilt. This leads to the temperature gradient being oriented southwest-northeastward. Therefore gridpoints east of the center point do not necessarily have higher values for the thickness of the atmospheric layer or the TFP. To overcome this, center points are compared with nine points to the northeast for the equivalent thickness condition, and six points to the east for the TFP-condition.

2.2.2. Detection on Isentropic Surfaces

Based on the work on the potential vorticity framework of cut-off lows by Hoskins et al. (1985), Wernli and Sprenger (2007) describe a contour searching algorithm used to identify the dynamical tropopause, defined as the 2 potential vorticity unit (PVU) isoline (with $1 \text{ PVU} \equiv 1 \times 10^{-6} \text{K kg}^{-1}$ $\text{m}^2 \text{ s}^{-1}$). The idea is to find two-dimensional regions of stratospheric air (PV > 2 PVU) that are fully embedded within tropospheric air (PV < 2 PVU).

Wernli and Sprenger (2007) performed their analysis on various isentropic levels, ranging from 295 to 360 K, separated by 5 K. For every level, starting at the equator and going poleward along a meridian, the first gridpoint with a PV-value greater than 2 PVU is being identified. Once the first high-value PV gridpoint is found all neighbouring gridpoints with PV-values greater than 2 PVU are being identified and attributed to the potential cut-off. This searching pattern is continued until the entire contour of the cut-off low is found. Structures which extend over the pole are being excluded, as these represent the main body of stratospheric air, and not an intrusion of stratospheric air into the troposphere.

Not all of the identified vortices with PV-values greater than 2 PVU are necessarily of stratospheric origin, as pointed out by the authors. Positive PV anomalies can also form from the release of latent heat due to condensation (Hoskins et al. (1985)). To distinguish cut-off lows from diabatically produced PV anomalies, feature tracking and testing for conservation of PV is required. It should be noted that Wernli and Sprenger (2007) omitted

these steps, as these additional operations are computationally very expensive. For lower isentropes some of the identified cut-off structures are also related to surface topography, and develop due to frictional processes near mountains (Thorpe et al. (1993)). Yet due to their stationarity it is possible to distinguish these structures from cut-off lows.

It is important to highlight that when detecting dynamical processes on isentropes one has to consider changes in the location of the isentropes themselves. Isentropic surfaces vary with season, time of day and latitude. Wernli and Sprenger (2007) for example found frequency maxima of PV structures on all isentropes, but with different locations depending on altitude. Therefore, caution must be exercised when considering seasonal cycles on isentropes. To consider the seasonality of isentropes, different isentropic levels must be used for PV feature detection, depending on the season and the region of interest (Nieto et al. (2008)).

2.2.3. Further Remarks

As opposed to a PV-based approach, detecting cut-off synoptic systems merely as closed contours on geopotential height maps does not account for its dynamics. As the cut-off condition is taken literally, the classification of a system from cut-off to non-cut-off can easily change, for example by advecting the whole system due to a uniform zonal flow, without changing the dynamics of the system significantly (Hoskins et al. (1985)). Within the conceptual model by Nieto et al. (2005) the cut-off criterion has been relaxed

to some extend, as only six of the eight neighbouring gridpoints must have greater geopotential height values than the central point.

Caution must be exercised when encountering absolute values of cut-off low occurrences on a spatial grid. While the conceptual model by Nieto et al. (2005) attributes by definition a limited number of gridpoints to a cut-off low event (by selecting the northernmost and westernmost gridpoint as the spatial representative of a cut-off low cluster), the PV approach by Wernli and Sprenger (2007) does not, leaving the possibility of many more gridpoints being attributed to a single event. In the case of Nieto et al. (2008), where the spatial distribution is given as number of occurrences per gridpoint, the PV approach thus detects more counts per gridpoint than the conceptual model approach by almost an order of magnitude.

2.3. Climatologies of Northern Hemisphere Cut-Off Lows

While there are multiple climatologies of Northern Hemisphere cut-off lows (for example Bell and Bosart (1989), Nieto et al. (2005), Wernli and Sprenger (2007), Muñoz et al. (2020)), direct comparison suffers from the usage of different cut-off low definitions, reanalysis data, vertical levels, time span, spatial and temporal resolution, and in general by a missing consensus on some of the core features regarding the structure of cut-off lows. One

uncertainty arises from the vertical location of the cold core, as previously mentioned by Pinheiro et al. (2020). An earlier study by Pinheiro et al. (2019) focuses on the sensitivity of cut-off lows to the detection scheme used. The authors analysed Southern Hemisphere cut-off lows at 300 hPa, and found that imposing a cold core condition significantly reduces cut-off low frequency, as compared to a detection scheme focusing solely on a cut-off condition using zonal and meridional wind fields. As the stratospheric air above a cut-off low is anomalously warm, detection schemes which impose a cold core condition might fail to detect systems at very high pressure levels, if the cold core is located in a deeper vertical level (Pinheiro et al. (2020)).

In the following section climatologies and associated characteristics of Northern Hemisphere cut-off lows will be presented. A strong focus will be put on the work of Muñoz et al. (2020). The authors applied an adapted version of the conceptual model by Nieto et al. (2005) consistently on two pressure levels, 200 and 500 hPa, in order to assess the sensitivity of cut-off low detection to the chosen pressure level.

Wherever discrepancies between the results of the original conceptual model by Nieto et al. (2005) and the adapted one by Muñoz et al. (2020) occur, it shall be mentioned. In order to consider multiple detection schemes, results from PV based detection schemes from Wernli and Sprenger (2007) and Nieto et al. (2008) will be discussed. However, direct comparison of the approaches is limited, as Wernli and Sprenger (2007) do not distinguish between stratospheric cut-offs and stratospheric streamers consistently, and

Nieto et al. (2008) put their main focus on the spatial distribution and seasonality of cut-off lows detected on isentropes, and do not consider features like trends or persistence.

2.3.1. Spatial Distribution

In the Northern Hemisphere, cut-off lows occur at three favoured regions: the northeastern Atlantic Ocean and southwestern Europe, the northeastern Pacific Ocean and western North America, and northeastern China-Siberia and northwestern Alaska, as depicted in Fig 2.2 (Muñoz et al. (2020)). There is a qualitatively good agreement among studies on the main regions of occurrence, not only for detection schemes based on the detection of geopotential height minima (Bell and Bosart (1989), Nieto et al. (2005)), but also for methods based on PV (Wernli and Sprenger (2007), Nieto et al. (2008)). Performing the detection of cut-off lows at a 500 hPa pressure level also highlights the northwestern Atlantic Ocean and the southern tip of Greenland as a region of high cut-off low occurrence (Bell and Bosart (1989), Muñoz et al. (2020)).

Regarding the movement of cut-off lows, Bell and Bosart (1989) describe cut-off lows as quasi-stationary. In contrast, Kentarchos and Davies (1998) found that about half of the detected cut-off lows lasting at least three days move considerably, with distances greater than 600 kilometers. This is in agreement with Nieto et al. (2005), though the two studies differ regarding the favoured direction of movement. While Kentarchos and Davies (1998)
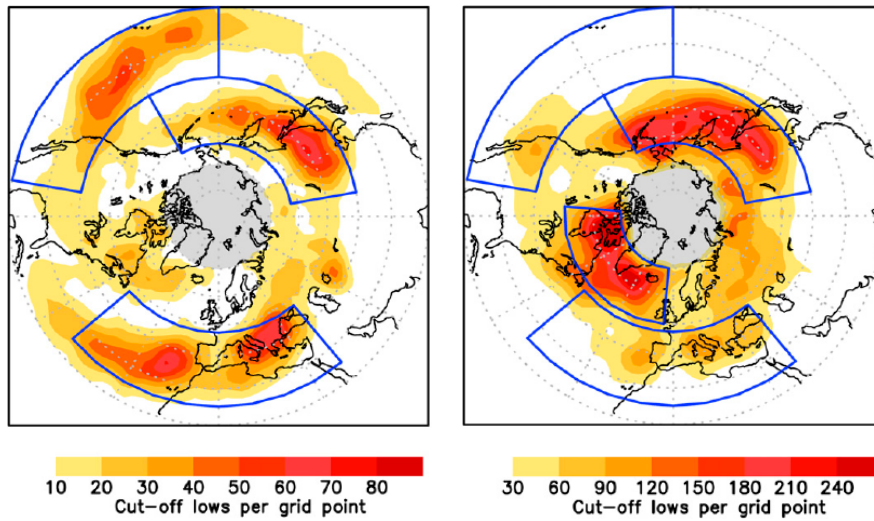
Figure 2.2.: Spatial distribution of cut-off lows detected on 200 hPa (left) and 500 hPa (right), on a 2.5° x 2.5° grid after a nine-point smoothing. Shading indicates the number of times between 1979 and 2017 that a gridpoint represented a cut-off low. Blue contours are favoured regions of occurrence. Note the difference in color-scaling. Adapted from Muñoz et al. (2020).

found that cut-off lows tend to move north- or northeastward as they decay, Nieto et al. (2005) describe a general trend for cut-off lows to move westward (except for certain regions such as Europe, where cut-off lows tend to move eastward within the first two days of occurrence).

2.3.2. Frequency, Persistence and Trends

Table 2.1 presents the number of detected cut-off lows between 1979 and 2017 by Muñoz et al. (2020). The increase in detected systems at 500 hPa

Number of cut-off lows (1979-2019)		
	200 hPa	500 hPa
North America	725	683
Europe	1234	2234
Asia	1115	3788
Greenland	562	3135
Northern Hemisphere	5136	13791

Table 2.1.: Number of cut-off lows events detected by Muñoz et al. (2020) in the Northern Hemisphere and the four favoured regions of occurrence, for 200 hPa and 500 hPa respectively. Based on table 2 from Muñoz et al. (2020).

compared to 200 hPa is consistent for all regions, except for North America, where the number of cut-off lows decreases when the detection is performed at 500 hPa. A possible explanation for the high level dependency given by the authors is that the occurrence of 500 hPa cut-off lows is not only driven by the strength of the subtropical jet, but also by the strength of the polar-front jet, acting as a waveguide for Rossby waves (as stated previously by Ndarana and Waugh (2010) for the Southern Hemisphere). Whether or not this level dependency might be a result of the imposed cold-core condition and therefore an artefact of the detection scheme, or a result of orographically induced cyclones at 500 hPa, has not been discussed by the authors.

Timeseries for Northern Hemisphere cut-off lows show strong signals of interannual variability (measured as standard deviation divided by mean) at the annual and seasonal scales, with the highest values found in North

America (39%), followed by Asia (23%) and Europe (20%) (Muñoz et al. (2020)). There is a discrepancy between studies when it comes to trends in the annual numbers of cut-off lows in the Northern Hemisphere. While Nieto et al. (2007) found no statistically significant trend, Muñoz et al. (2020) found a positive trend of cut-off low occurrence, for both 200 and 500 hPa. The increase in number is larger for 500 hPa, though the difference between the 200 and 500 hPa slopes is not statistically significant, except for North America. No trend analysis has been performed using a PV based detection scheme.

Cut-off lows are short-lived events, which is well represented by climatologies. Around 80% of the detected cut-off low events in Muñoz et al. (2020) persist equal or less than 72 hours, and 5% last more than 5 days. Furthermore, cut-off lows detected on 500 hPa tend to be more persistent than systems detected at 200 hPa.

2.3.3. Seasonality

In the recent work of Muñoz et al. (2020) cut-off lows show a level dependent seasonality (see Fig 2.3). For the 200 hPa pressure level, the most events occur in summer, and the least events take place in winter, consistent with the seasonal variability of the strength of the jetstream. The 500 hPa cut-off lows show no seasonality, except for the case of North America, where cut-off low occurrence decreases towards summer. A summer minimum in

western North American 500 hPa cut-off lows has also been documented by Bell and Bosart (1989).

The seasonality of upper-level cut-off lows is consistent among detection schemes. Nieto et al. (2008) additionally presents the monthly distribution of cut-off lows detected on isentropic surfaces at 320 and 340 K. For both levels the number of cut-off low occurrence is highest in summer and lowest in winter, with a higher amplitude for the monthly cycle for the 340 K level.
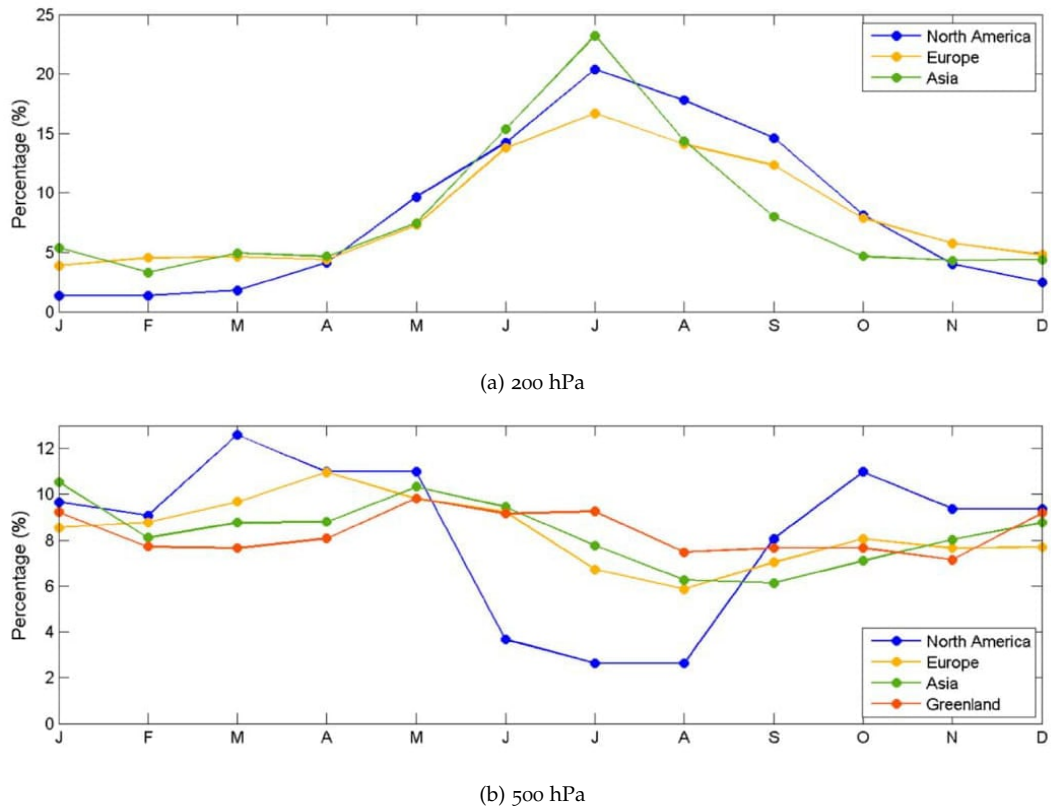
(a) 200 hPa

(b) 500 hPa

Figure 2.3.: Annual cycle of 200 hPa (top) and 500 hPa (bottom) cut-off lows in the main regions of occurrence for the period 1979 to 2019. Note the difference in scale, adapted from Muñoz et al. (2020).

3. Methods

While previous studies agree on some statistics of cut-off lows in the Northern Hemisphere, such as the duration and the spatial distribution, there are significant differences in terms of frequency and seasonality at different pressure levels. The usage of different cut-off low definitions and detection schemes poses uncertainties in terms of the comparability of results among studies.

In this chapter a new method for cut-off low identification and tracking will be presented. This approach omits additional assumptions about cut-off low structure, and focuses on the principal definition of a cut-off circulation at upper tropospheric levels.

3.1. Introducing TRACK

The climatologies presented in section 4 are based on the feature detection and tracking software TRACK (Hodges (1994, 1995, 1999)). TRACK has

previously been used as a cyclone detection tool in a variety of applications, regions, and datasets. Some examples are the assessment of projected changes in extratropical cyclones and associated precipitation in CMIP5 models (Zappa et al. (2015)), seasonal forecasting of tropical cyclone activity (Manganello et al. (2014)), or the analysis of Arctic storms in reanalysis data (Vessey et al. (2020)). Recently, Pinheiro et al. (2017, 2019, 2020a, 2020b) used a modified version of TRACK to detect cut-off low systems at 300 hPa in the Southern Hemisphere, by applying additional filters to ensure a cut-off circulation.

The detection of synoptic-scale systems within TRACK is performed in three steps: segmentation, feature point detection and solving of the correspondence problem. These terms are widely used in digital image processing and computer vision, and already point towards the idea of treating the detection of synoptic features as an image recognition problem. In order to identify and track synoptic systems, a suitable field and the region of interest first have to be defined. In the case of cyclones this is usually the geopotential or the vorticity field.

Once the region of interest is specified, segmentation can be initiated. Segmentation is the process of dividing the field into different parts/segments, in the case of TRACK into *objects* and *background*. For that, a threshold must be chosen, which divides the field into objects, if the intensity at the grid point is greater than the threshold, and background if the intensity is below the threshold. A full description of the segmentation process can be found in Hodges (1994).

The feature point detection can either be performed on a conformal cylindrical projection (Hodges (1994)), or on a unit sphere (Hodges (1995)). Suitable feature points are usually local extreme values. TRACK is able to compute the off-grid local maxima or minima, based on an interpolation/smoothing (after Dierckx (1981, 1984)) and local maximization approach (after Goldfarb (1969)), which improves track smoothness in low resolution data. As the field has previously been decomposed into objects and background, the computationally expensive process of field interpolation/smoothing can be restricted to the predefined object spaces. The local maximization algorithm returns the position and the field values (for example intensity) of the local extreme values, which are for each frame separately stored as feature points.

The last step is to track the feature points in consecutive time frames and determine their correspondence, also known as solving the correspondence problem. Within TRACK this is treated as a constrained optimization of a cost function, and is based on the idea that the motion of objects can not change instantaneously. Instead, the velocity is expected to change smoothly within consecutive frames. The cost function is therefore constructed from measures of local track smoothness, which are changes in direction and speed. The goal is to find the set of tracks that minimize the cost function, and maximize the track smoothness. This is achieved by swapping points along tracks, so as to gain the maximum smoothness. The presentation of the full algorithm is omitted here, but can be found in appendix A.

Hodges (1999) presents an extension to TRACK, which introduces adaptive

constraints for the feature tracking. These constraints come in the form of a regional upper-bound displacement and an adaptive track smoothness constraint. The upper bound displacement (d_{max}) dictates the maximum allowed displacement within two time steps, and is defined for a latitudinal range (Pinheiro et al. (2019)). The track smoothness constraint is a measurement of changes in direction and speed, and is to be set according to the expected motions of the system. It is specified by an upper-bound value (Ψ_{max}), which is a function of the mean displacement distance over three consecutive time steps ($\bar{d}$).

These adaptive constraints enable a wide range of systems to be detected and tracked. The next section will focus on how to use TRACK in order to detect mid-latitude cut-off lows in the Northern Hemisphere.

3.2. Cut-Off Low Detection with TRACK

Two cut-off low climatologies have been obtained for a 41-year period (1979-2019) using the ERA5 reanalysis dataset (Hersbach et al. (2020)), with a spatial resolution of 0.25°x0.25°, and a temporal resolution of six hours. The detection and tracking has been performed with TRACK version 1.5.2., and is based on the work of Pinheiro et al. (2019), who applied the same detection scheme in the Southern Hemisphere. The tracking consists of two steps, which are the detection of low pressure systems at 300 hPa, and the additional filtering to exclude open troughs. This is consistent with the

cut-off low definition presented by Palmén (1949), who defines a cut-off low as a cyclonic circulating system in the upper troposphere detached from the westerlies. In contrast to the work of Nieto et al. (2005) or Muñoz et al. (2020), no cold-core criteria is applied. Northern Hemisphere cut-off lows northward of 20° latitude and southward of 70° latitude have been identified.

Detection and tracking of feature points has been performed on two fields, the 300 hPa geopotential (Z_{300}) and the 300 hPa relative vorticity (ξ_{300}) fields. Zonal and meridional winds at 300 hPa have been used for the additional filtering for a cut-off circulation.

3.2.1. Preprocessing

The geopotential field is dominated by large spatial scales. In order to reduce the influence of the large-scale background field on the detection of feature points, the zonal mean is removed from the Z_{300} field. Further analysis is being performed on the geopotential anomaly field (Z'_{300}). This has the advantage that weak local extremes can more easily be identified, especially at lower latitudes where the geopotential gradient is usually weaker (Pinheiro et al. (2019)). Also, a spherical harmonic decomposition has been performed on Z'_{300} and ξ_{300}, setting wavenumbers less than or equal to five to zero.

Relative vorticity is in general less influenced by the background field, but the field can be noisy in high resolution data. This is a consequence of relative vorticity being dependent on higher-order derivates, resulting in the enhancement of smaller spatial scales (Hoskins and Hodges (2002)). Some sort of smoothing is therefore required. For that the data is spectrally truncated to triangular truncation 42 (T42) on a Gaussian Grid for relative vorticity, and T63 for the geopotential. Different truncation numbers are used to provide a fairer comparison of the two fields and their associated spatial scales, similar to Pinheiro et al. (2019).

3.2.2. Detection and Tracking

First, potential feature points in both fields are identified. These are defined as minima below -50 gpm for Z'_{300}, and maxima greater than $1.0 \times 10^{-5} s^{-1}$ for ξ_{300}. The number of detected systems is sensitive to these thresholds. Increasing their magnitudes results in fewer systems being detected, as weaker features are being excluded.

In the next step an initial set of tracks from the detected feature points are constructed using a nearest neighbour approach. This first set of tracks then gets refined by minimizing the cost function. The adaptive constraints used to detect cut-off lows are shown in table 3.1, adapted from Pinheiro et al.

Zonal upper-bound displacements			
Zones j	1	2	3
Lower (deg lat)	-90.0	-20.0	20.0
Upper (deg lat)	-20.0	20.0	90.0
d^j_{max} (°)	3.0	3.5	3.0
Adaptive track smoothness			
$\bar{d}$ (deg)	1.0	3.0	6.0	> 8.0
Ψ_{max} ($\bar{d}$)	1.0	0.3	0.1	0.01

Table 3.1.: Adaptive constraints used for feature point tracking

(2019)[1]. The displacement of systems in the region of interest is constrained to a distance of $d_{max} = 3°$ within 6 hours, reflecting the stationarity of cut-off lows. The values for the upper-bound track smoothness constraint Ψ_{max} are presented in the last row of 3.1. High values for the mean displacement in three consecutive frames ($\bar{d}$) are linked to low values of Ψ_{max}. In other words, the track smoothness constraint is more restrictive if the feature points are further apart, and vice versa.

3.2.3. Post-Tracking Filtering

Systems lasting at least 24 hours were retained, and further tested for a circulation cut-off from the main westerly flow. For that, a four-point wind

---

[1]Pinheiro et al. (2019) define an upper (lower) latitudinal boundary for zone 1 (2) of -15 degrees latitude. As the current work tracks cut-off lows only on the Northern Hemisphere, these adjustments have no effect on the present analysis.

filter has been applied to the feature points. The zonal and meridional wind fields are sampled at a radial distance of 5° from the feature point in four directions (offset points), as depicted in Fig. 3.1. In order to exclude open troughs from the climatology, the wind directions at the offset points have to reveal a cyclonic circulation around the feature point. To be specific, the following conditions have to be satisfied: $u_{0°} < 0$ (where $u_{0°}$ is the zonal wind at the offset point of 0° relative to North), $v_{90°} > 0$ (with $v_{90°}$ being the meridional wind at 90° relative to North), $u_{180°} > 0$ and $v_{270°} < 0$.

$$ u < 0 $$

$$ 0° $$

$$ v < 0 \quad 270° \quad \xi_{max} \text{ or } Z'_{min} \quad 90° \quad v > 0 $$
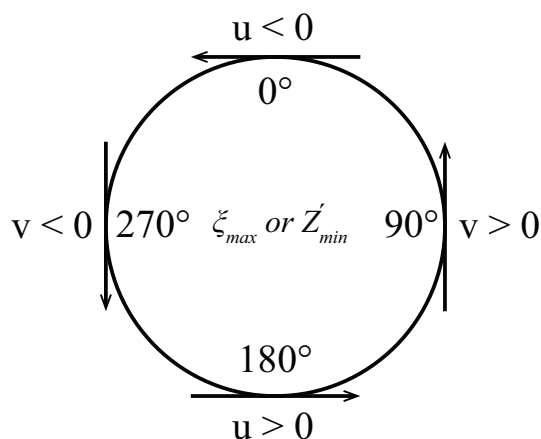
$$ 180° $$

$$ u > 0 $$

Figure 3.1.: Schematic representation of the 300 hPa horizontal four-point wind filter, applied to previously detected feature points of either ξ_{max} or Z'_{min} at a radial distance of 5°. Based on Fig. 1 in Pinheiro et al. (2019), but adjusted to represent cyclonic circulation in the Northern Hemisphere.

Only those systems satisfying the conditions for at least four consecutive frames (24 hours) were retained. If the criteria imposed by the four-point filter was not met on one frame, but then again for the following four consecutive frames, the track was split and the systems were analysed as

two separate cut-off low events, even though the second one potentially originated from the first one.

4. Results

4.1. Frequency, Trends and Spatial Distribution

The climatologies both obtained from Z'_{300} and ξ_{300} show strong internal variability, as presented in Fig. 4.1 (note the difference in scale). In terms of absolute number of events, tracking on ξ_{300} yields more events than tracking on Z'_{300}, with 40737 events detected for ξ_{300} and 24912 events for Z'_{300} respectively. Both climatologies show a positive trend for the considered timespan, though the trend is more pronounced in ξ_{300}. Following a least squares regression line, the increase of cut-off low events per year is $+1.99$ for ξ_{300}, and $+0.44$ for Z'_{300}. The Root Mean Square Error (RMSE) has also been calculated as a measure of how well the regression line fits the original data. RMSE values are 28.58 for ξ_{300} and 18.70 for Z'_{300} (in units *events per year*). Normalizing by the mean of the observations yields only small differences among fields, with a Normalized Root Mean Square Error (NRMSE) of 0.0288 for ξ_{300} and 0.0308 for Z'_{300}, indicating similar magnitudes of interannual variability.

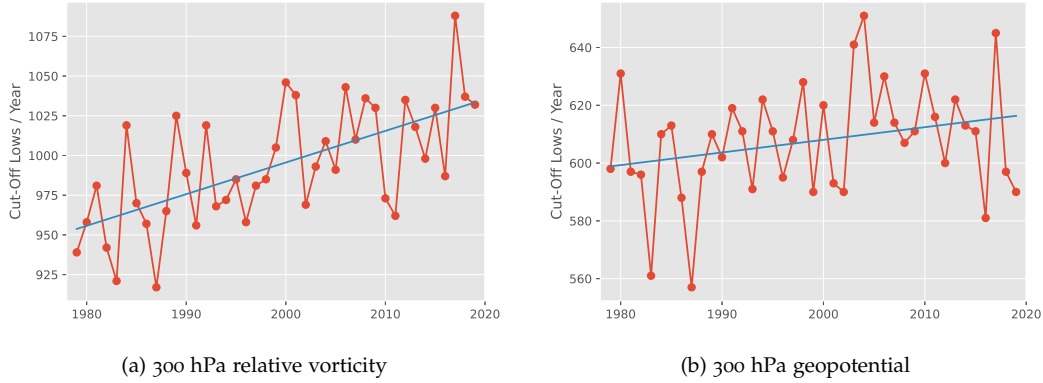(a) 300 hPa relative vorticity

(b) 300 hPa geopotential

Figure 4.1.: Interannual variability of 300 hPa cut-off lows for the climatologies (a) ξ_{300} and (b) Z'_{300} for the period 1979-2019. Blue line represents the least squares regression line, with a slope of (a) +1.99 events/year and (b) +0.44 events/year. Note the difference in scale.

The number of annual cut-off lows events has also been analysed for regions of favoured occurrence seperately, see Fig. 4.2. To improve comparability among studies, the region borders are the

Asia	40°N to 62.5°N	100°E to 150°W
Europe	25°N to 47.5°N	50°W to 40°E
Greenland	50°N to 70°N	95°W to 5°W
North America	20°N to 40°N	100°W to 180°

Table 4.1.: Latitudinal and longitudinal range of the favoured regions of cut-off low occurrence used in the present work. Adapted from Muñoz et al. (2020).

same as in Muñoz et al. (2020), see table 4.1. The number of detected systems in Z'_{300} is lower for every region, compared to ξ_{300} (except for Greenland in winter, see table 4.3). For Z'_{300} most events are detected in Asia (20%), followed by Europe (18%), Greenland (13%) and North America (12%). If tracking is performed on ξ_{300} most events are detected in Europe (15%) and Asia (14%), followed by North America (11%) and Greenland (9%).
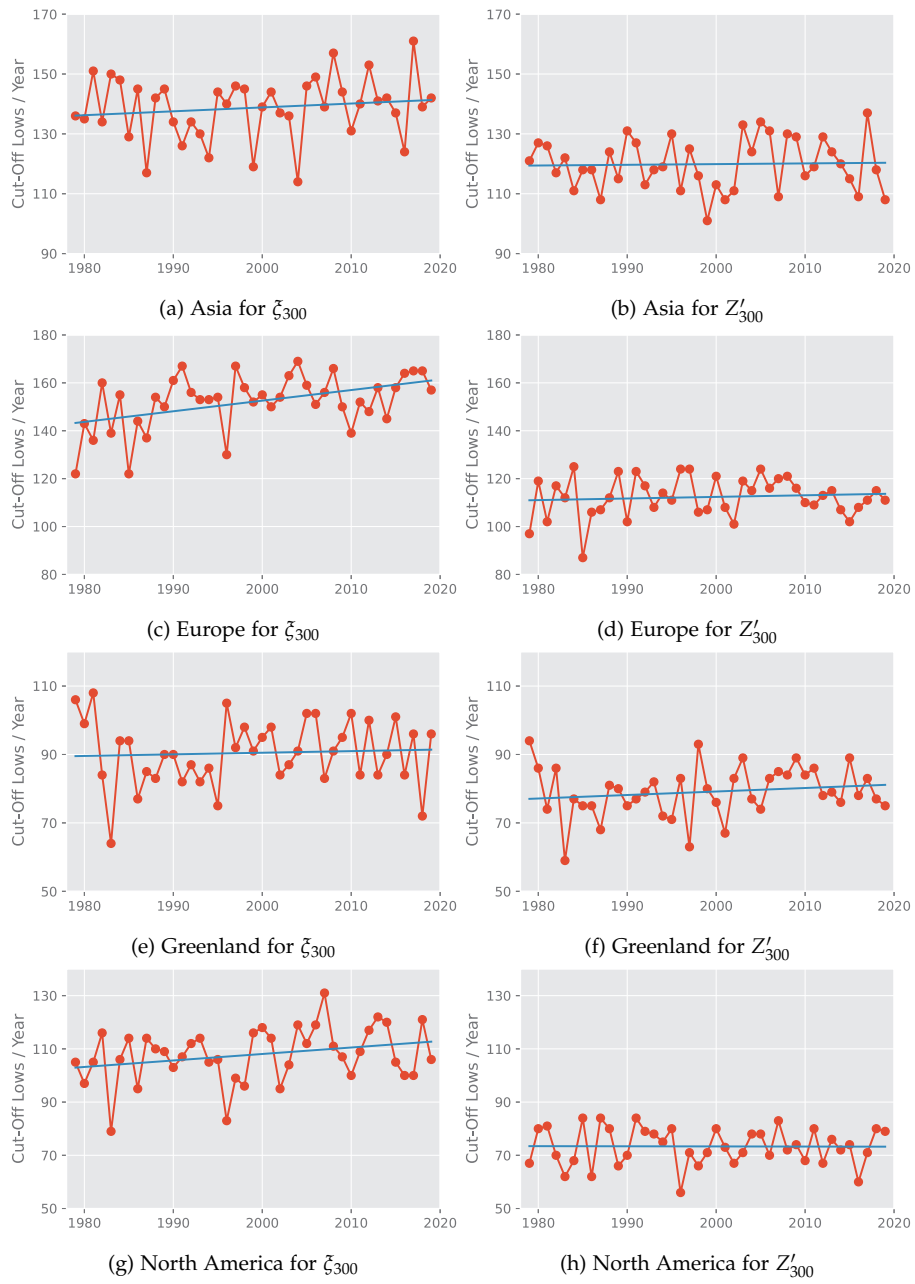
Figure 4.2.: Interannual variability of 300 hPa cut-off lows between 1979 and 2019 for the climatologies ξ_{300} (left) and Z'_{300} (right) for favoured regions of occurrence separately. Blue line represents the least squares regression line. Note the difference in scale among regions.

As the Asian and the North American domain share a border it is possible for an event to take place at both domains, but in different frames, if the system is advected across the shared border. In those cases the location of the first occurrence determines the attribution of a cut-off low to a certain region, in order to avoid a system being analysed several times. Testing the sensitivity of this definition, 81 events for Z'_{300} and 95 events for ζ_{300} have been attributed to Asia, but not to North America. Also, 163 events for Z'_{300} and 190 events for ζ_{300} have been attributed to North America, but not to Asia respectively. As these numbers are small compared to the total number of detected events, no major distortion on the derived regional metrics are expected.

Trends are also calculated for the four favoured regions of cut-off low occurrence, presented in table 4.2. The increase in cut-off low occurrence is stronger for ζ_{300} in every region, except for Greenland. The most pronounced difference in trends is found for the European region, where tracking on ζ_{300} yields an increase in events of $+0.44$ per year, and $+0.07$ for tracking on Z'_{300}. Also, over the entire timespan North America does not experience an increase in annual events for Z'_{300}, while it does for ζ_{300} ($+0.24$ events per year).

The increase in annual events with time is not limited to the main areas of cut-off low occurrence. For both climatologies, 57% of the trend observed for the entire domain is not attributable to any of the favoured region of occurrence, but observed outside of these boundaries. For Z'_{300} 9143 events (37%) do not enter any of the prescribed regions, and for ζ_{300} the number is

Trend of annual number of cut-off low occurrence (1979-2019)						
	NH	Asia	Europe	Greenland	North America	Other
Trend (ξ_{300})	+1.99	+0.13	+0.44	+0.05	+0.24	+1.13
NRMSE (ξ_{300})	0.029	0.073	0.066	0.105	0.090	0.040
Trend (Z'_{300})	+0.44	+0.02	+0.07	+0.10	0.00	+0.25
NRMSE (Z'_{300})	0.031	0.071	0.073	0.091	0.095	0.067

Table 4.2.: Trend of annual number of cut-off lows (1979-2019) in unit events per year, for the entire Northern Hemisphere (NH) and regions defined in table 4.1. The last column (*Other*) contains those events not attributable to any of the four favoured regions of occurrence.

even higher with 20683 events (49%). Taking a look at the spatial distribution, Fig. 4.3 highlights the occurrence of cut-off lows in areas not previously mentioned in other studies. For both fields Z'_{300} and ξ_{300} one of those areas is Central Asia, east of the Caspian Sea. Noteworthy is also the occurrence of cut-off low events southwest of the European region over the Atlantic Ocean, as well as the region around 20°N latitude in the Pacific Ocean, particularly pronounced in the ξ_{300} climatology.

4.2. Seasonality

To consider the seasonality of cut-off lows, Fig. 4.4 shows the spatial distributions of events for different seasons (MAM - spring; JJA - summer; SON - autumn; DJF - winter). Consistent with the change in the meridional temperature gradient and the strength of the jet stream among seasons,

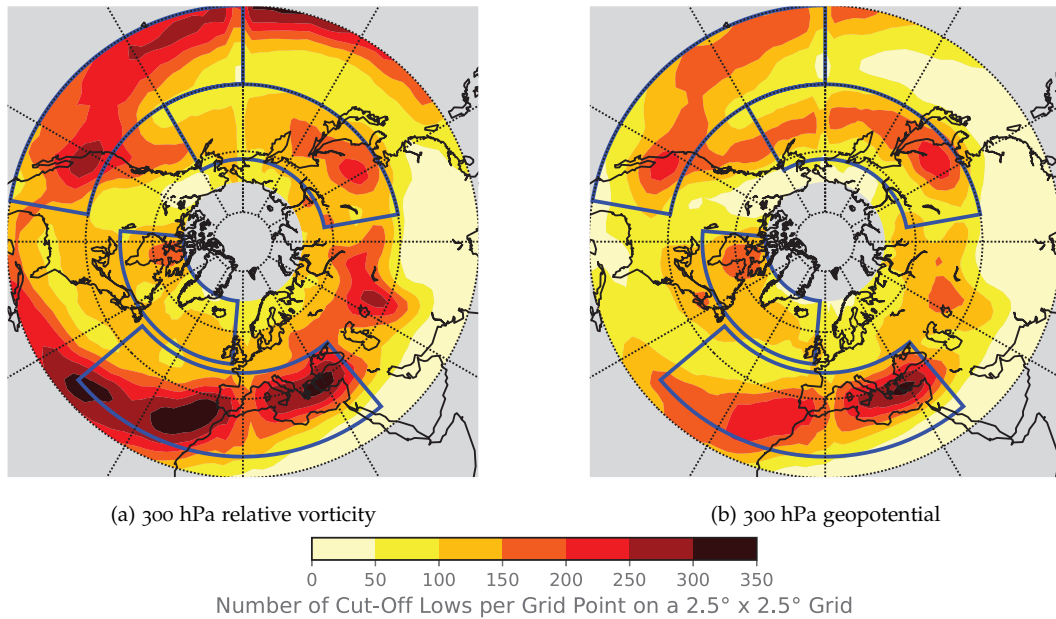(a) 300 hPa relative vorticity   (b) 300 hPa geopotential

0   50   100   150   200   250   300   350
Number of Cut-Off Lows per Grid Point on a 2.5° x 2.5° Grid

Figure 4.3.: Spatial distribution of 300 hPa cut-off lows, detected on (a) ζ_{300} and (b) Z'_{300}, for the entire period of 1979-2019. Cut-off low locations have been interpolated on a 2.5° x 2.5° grid, after a nine-point smoothing. Shading indicates the number of times between 1979 and 2019 a gridpoint was part of a cut-off low, grey shaded areas are regions excluded from the analysis. Blue contours represent the domains of favoured cut-off low occurrence, which are adapted from Muñoz et al. (2020).

winter and summer patterns differ the most, with spring and autumn representing a transition between these two seasons. The spatial distribution, as well as the magnitudes of cut-off low occurrence in spring (Fig. 4.4a and 4.4e) and winter (Fig. 4.4d and 4.4h) show strong similarities among the two climatologies, with most cut-off lows occurring in Europe and the southwestern coast of North America. The spatial distributions diverge in summer among climatologies (Fig. 4.4b and 4.4f), when previous studies found the highest rates of cut-off low occurrence. This is the time when

cut-off lows in the ξ_{300} climatology develop at the previously mentioned low latitudes in the Atlantic and Pacific Ocean, outside of the European and North American domain. For both climatologies, the transition from spring to summer shifts the previously detected southwestern North American maximum to a higher latitude outside of the domain, and gives rise to a new maximum in the central Pacific Ocean. Summer also enhances the spatial distribution of cut-off lows over the northwestern Pacific Ocean, where other seasons show rather low magnitudes. Autumn represents the transition from summer to winter, therefore still showing some of the pronounced summer patterns, but experiencing a decrease in magnitude.

It shall be mentioned that the spatial distribution plots not only depend on the number of cut-off lows detected, but also on their individual duration. As the color scaling indicates the times a cut-off low occurred at a certain gridpoint, the pattern produced by a set of five events each lasting two days can be the same as the pattern produced by a set of two events each lasting five days. It is therefore not correct to conclude from Fig. 4.4 alone that more events occur in summer, compared to other seasons.

Fig. 4.5 gives an accurate view on the seasonality of cut-off lows. For the ξ_{300} climatology, a pronounced summer maximum and winter minimum is present for Northern Hemisphere cut-off lows, as well as cut-off lows attributed to Asia and Greenland. North America follows the same pattern, though the seasonality is less pronounced, and the number of events decreases in June. Europe is the only region where more events have been
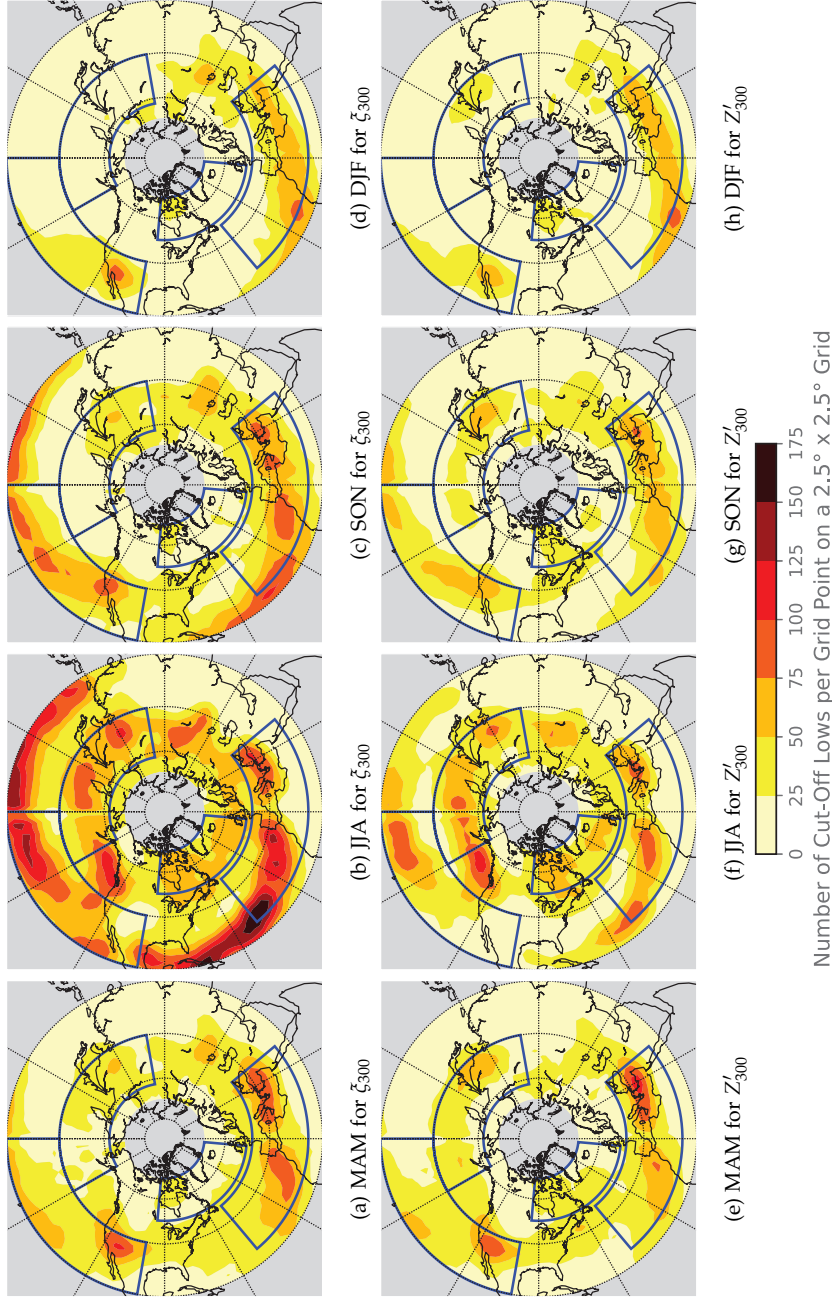
(a) MAM for ζ_{300} (b) JJA for ζ_{300} (c) SON for ζ_{300} (d) DJF for ζ_{300}

(e) MAM for Z'_{300} (f) JJA for Z'_{300} (g) SON for Z'_{300} (h) DJF for Z'_{300}

Number of Cut-Off Lows per Grid Point on a 2.5° x 2.5° Grid

Figure 4.4.: Seasonal distribution of ζ_{300} cut-off lows (top) and for Z'_{300} cut-off lows (bottom), for season spring (MAM), summer (JJA), autumn (SON) and winter (DJF). Cut-off low locations have been interpolated on a 2.5° x 2.5° grid, after a nine-point smoothing. Shading indicates the number of times between 1979 and 2019 a gridpoint was part of a cut-off low, grey shaded areas are regions excluded from the analysis. Blue contours represent the domains of favoured cut-off low occurrence (adapted from Muñoz et al. (2020)).

Cut-off Low Occurrence per Season (1979-2019)							
	ξ_{300}				Z'_{300}		
	MAM	JJA	SON	DJF	MAM	JJA	SON	DJF
NH	9836	13542	10380	7069	6572	7266	6354	4720
Asia	1398	2262	1293	734	1326	1627	1253	709
Europe	1676	1669	1636	1256	1340	1060	1174	1031
Greenland	822	1568	840	479	732	1161	787	562
North America	1119	1281	1170	851	908	583	785	731
Other	4821	6762	5441	3749	2266	2835	2355	1687

Table 4.3.: Cut-off low occurrence between 1979 and 2019 for each season and region separately, for the ξ_{300} climatology (left) and the Z'_{300} climatology (right). *Northern Hemisphere* (NH, top line) represents detected events over the entire domain (20°N to 70°N); *Other* (bottom line) contains those events not assignable to any of the prescribed regions of favoured cut-off low occurrence in table 4.1.

detected in spring than in summer, with most events occurring in May, cut-off low occurrence decreasing from May to July, and increasing again until October. Table 4.3 gives the absolute number of cut-off low occurrence grouped by seasons, highlighting the prevalent winter minimum, and varying amplitudes of seasonality depending on the region.

Taking a look at the Z'_{300} climatology, most Northern Hemisphere cut-off lows occur in May, with number of events decreasing until February. Asia shows a similar distribution, with a maximum in May, and a minimum in January. Greenland experiences the same summer maximum and winter minimum as it does in the ξ_{300} climatology, with the most events taking

place in July, and the least in January. What is interesting are the seasonal distributions for Europe and Greenland in the Z'_{300} climatology. Both regions experience a spring-maximum in cut-off low occurrence, followed by another maximum in autumn, while the least events occur in July for the North American domain, and August for the European domain.
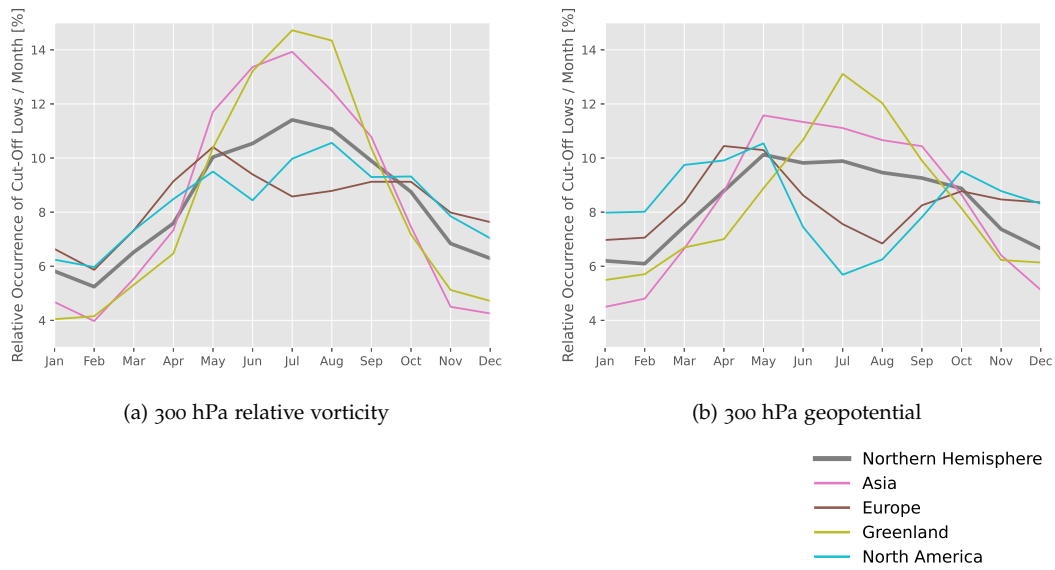

(a) 300 hPa relative vorticity   (b) 300 hPa geopotential

Figure 4.5.: Relative occurrence of 300 hPa cut-off lows for (a) ξ_{300} and (b) Z'_{300} for the period 1979-2019 expressed as percentage of the total number of cut-off low events that occurred within each month.

4.3. Persistence and Intensity

Both climatologies highlight the relatively short lifetimes of cut-off lows (Fig. 4.6). Most cut-off lows last less than two days, with number of events de-
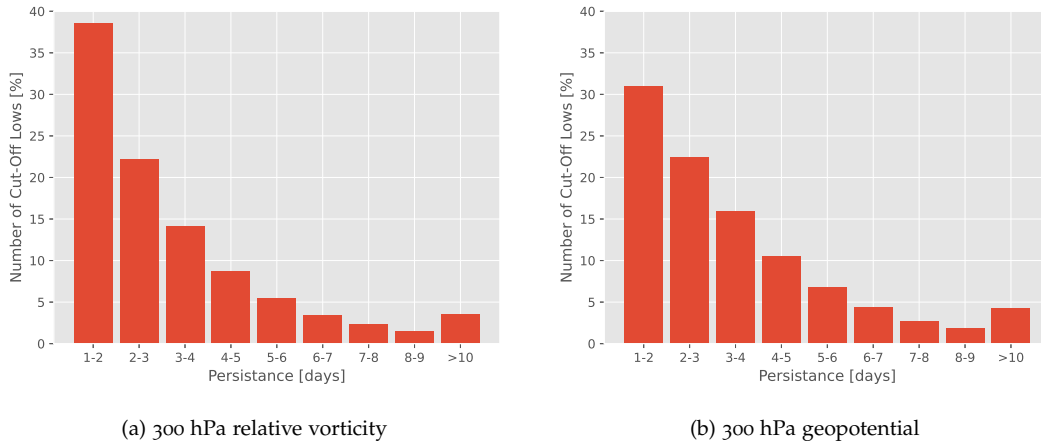
(a) 300 hPa relative vorticity

(b) 300 hPa geopotential

Figure 4.6.: Duration of cut-off lows for the climatologies (a) ξ_{300} and (b) Z'_{300} for the period 1979-2019, in unit days. Systems lasting less than 24 hours have been excluded from the analysis.

creasing monotonically for longer lived events. The main difference among climatologies is that 39% of the ξ_{300} events last less than two days, while only 31% percent of Z'_{300} cut-off lows last less that two days. In return, the fraction of events lasting more that two days is consistently higher in Z'_{300}, compared to ξ_{300}.

When taking a look at the persistence of events for the favoured regions of occurrence separately, a more detailed view emerges (Fig. 4.7). Typical durations of events are similar among climatologies for the four predefined regions. It is mainly for the events not attributable to a specific region that the fraction of very short lived events (less than 48 hours) is higher for the ξ_{300} climatology, than for the Z'_{300} climatology.

Finally, the seasonal intensity distributions have been computed, and are pre-

(a) 300 hPa relative vorticity
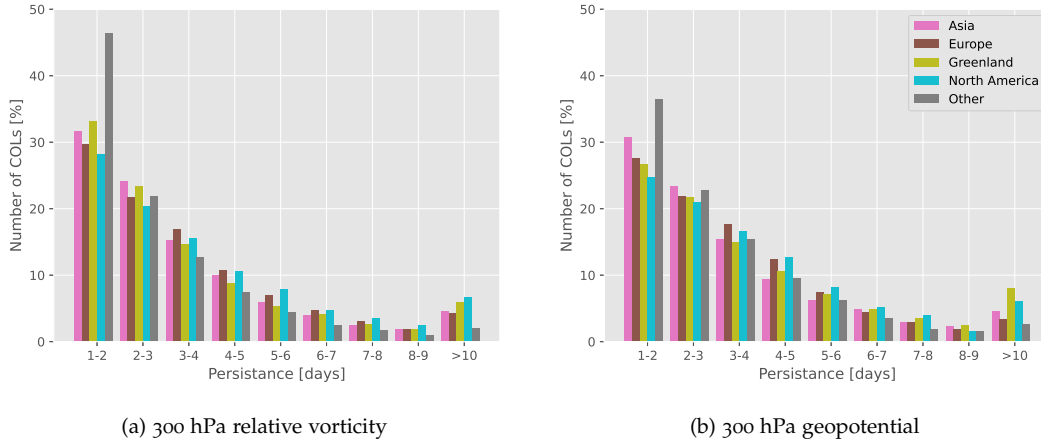
(b) 300 hPa geopotential

Figure 4.7.: Duration of cut-off lows for the climatologies (a) ζ_{300} and (b) Z'_{300} for the period 1979-2019, separated by regions, in unit days. Systems lasting less than 24 hours have been excluded from the analysis.

sented in Fig. 4.8. The most intense Z'_{300} cut-off lows are found in winter and autumn, followed by spring and summer. For ζ_{300}, spring, autumn and winter show similar distributions of very intense cut-off lows ($> 15 \cdot 10^{-5} s^{-1}$), with a higher number of medium-intensity events in spring, compared to autumn and winter. The least-intense events occur in summer.

4.4. Discussion

Comparing the annual number of cut-off lows derived from the current work with the numbers obtained from Muñoz et al. (2020) highlights the detection of more events for the same domain when using TRACK. Muñoz et al. (2020) detect roughly between 90 (280) and 160 (400) events per year at
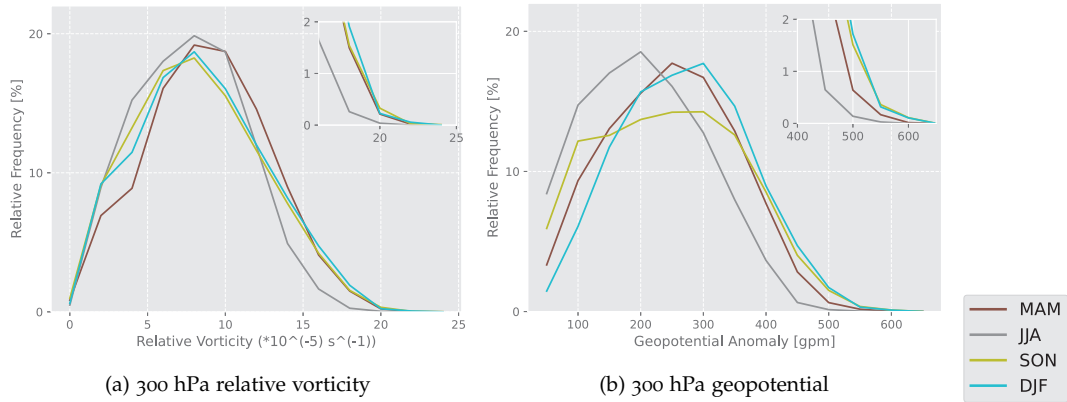
(a) 300 hPa relative vorticity   (b) 300 hPa geopotential

Figure 4.8.: Seasonal intensity distributions for the climatologies (a) ξ_{300} in units $10^{-5}s^{-1}$ and (b) Z'_{300} in units gpm for the period 1979-2019.

a 200 (500) hPa geopotential surface over the entire Northern Hemisphere. When excluding systems lasting between 24 and 36 hours, as done by Muñoz et al. (2020), using TRACK yields in average 760 events per year for ξ_{300}, and 497 events per year for Z'_{300}. It was to be assumed that the number of events is going to be higher for the present work, because the chosen method is per definition less restrictive, as it only assumes a cyclonic circulation around the local minimum and no additional restrictions like a present cold core or a front east of the center. The difference in number highlights the sensitivity of cut-off low systems to the detection scheme (and therefore the cut-off low definition used), similar to cut-off lows in the Southern Hemisphere (Pinheiro et al. (2019)). To quantify which definition represents cut-off lows better, and if the number of cut-off lows is overestimated in the present work, or underestimated in previous studies, visual inspections of geopotential height maps are necessary and should be considered for future work. Also, the sensitivity in feature point detection to the prescribed threshold (in the

current work -50 gpm for Z'_{300} and $1.0 \times 10^{-5} s^{-1}$ for ξ_{300}) should be further analysed to investigate if higher thresholds alter the structure of detected cut-off lows.

One of the main differences between the two derived climatologies is the difference in number of detected cut-off lows. Tracking on ξ_{300} detects more events per year than tracking on Z'_{300}. This is in accordance with Pinheiro et al. (2019), who used the same cut-off low detection scheme in the Southern Hemisphere, and who also found more tracks for the ξ_{300} climatology, compared to the Z'_{300} climatology. According to the authors the differences amongst climatologies are highest at lower latitudes and during summer months, when the geopotential gradient at lower latitudes is weak. Similar conclusions can be derived from the present study. Considering the seasonal and spatial distribution, it is reasonable to assume that the higher number of cut-off low events in the ξ_{300} climatology are a result of summer cut-off lows occurring between latitudes 20°N and 30°N within the central Atlantic and Pacific ocean in the ξ_{300} climatology, but not the Z'_{300} climatology.

The spatial distribution of cut-off lows obtained in the present work also highlights Central Asia as a region of high cut-off low occurrence, which has not been mentioned as a region of favoured occurrence by neither Nieto et al. (2005), nor Muñoz et al. (2020). The present finding of cut-off low occurrence over Central Asia is in agreement with Guo et al. (2021), who used a cut-off low detection scheme based on tracking minima in the 500 hPa geopotential height field. The authors also investigated the vertical

structure of cut-off lows over the region of interest (60–90°E, 35–55°N), and found a pronounced warm core of the systems at 200 hPa. This warm core explains why the region is not identified in the previously mentioned studies, and emphasizes the deficiency of assuming a cold core at very high pressure levels. In terms of spatial distribution, TRACK offers a potential alternative in detecting cut-off lows, as tracking can be performed at high pressure levels (where cut-off lows develop, and orographically induced systems are not dominant).

Muñoz et al. (2020) also mention Greenland as a region of favoured cut-off low occurrence, when tracking is performed at 500 hPa. While the present work detects cut-off low occurrence over the domain of Greenland, the pattern of spatial distribution is less pronounced in the present analysis (see Fig 9a in Muñoz et al. (2020)). The authors detect more cut-off low events over Greenland for the period 1979-2017, than over Europe and North America combined, if tracking is performed at 500 hPa.

The defined regions of favoured cut-off low occurrence presented in table 4.1 were directly adopted from Muñoz et al. (2020) in order to improve comparability among studies. The borders fit the present results only to some degree. Especially the European and the North American border cuts through dense cut-off low areas (see Fig. 4.3), potentially distorting domain-specific information, e.g. the regional pattern of seasonality or the absolute number of events and trends. For full disclosure it has to be mentioned that derived regional information might be sensitive to the chosen area, especially for Europe and North America.

The Z'_{300} and ξ_{300} climatologies not only differ in terms of annual events, but also in terms of linear trends. While both climatologies show an increase of annual events over the observed period, the trend is clearer in the ξ_{300} climatology. The direction of change is in agreement with Muñoz et al. (2020), though the magnitudes differ.

In accordance with previous studies, cut-off lows from both climatologies are short-lived events. A higher fraction of events lasting less than 48 hours are present in the ξ_{300} climatology, especially for locations not yet associated with high cut-off low occurrence. According to various studies on cyclone detection (e.g. Hoskins and Hodges (2002)), systems can be detected sooner in their lifetime if tracking is performed on the relative vorticity field, as the field is less influenced by the large-scale background flow. It is therefore possible that the higher number of very short-lived events in the ξ_{300} climatology is a result of detecting events sooner in their lifetime, and attributing them a duration of more than 24 hours, while the same event is attributed a duration less than 24 hours in the geopotential field. Some very short-lived events are therefore excluded in the Z'_{300} but not the ξ_{300} climatology, as they fall below the minimum lifetime restriction of 24 hours, which to some extend might aso explain why the ξ_{300} climatology contains more cut-off low events than the Z'_{300} climatology.

In terms of duration, it is also possible that the adaptive constraints defined in section 3.2 are too restrictive for cut-off low systems in the Northern Hemisphere. As an example, allowing a higher upper-bound displacement d_{max} can lead to a decrease in the absolute number of events and an increase

in their duration. By allowing feature points in consecutive frames to be further apart, cut-off lows previously treated as two separate events might be counted as one merged event (and vice versa).

This trade-off between number of events and their individual duration might also explain to some extent the detected decrease in cut-off low occurrence over the European and North American domain during summer. The spatial distribution of cut-off low occurrence for each season (see Fig. 4.4) does not indicate a strong decline in cut-off low density in summer compared to other seasons for the European or the North American domain. To give an example: the seasonality over the North American domain in the Z'_{300} climatology (Fig. 4.5b, blue line) shows a global minimum in cut-off low occurrence in summer. Intuitively one would expect an associated decrease in the spatial distribution of cut-off low occurrence. However, considering the spatial distribution for summer (Fig. 4.4f) and winter[1] (Fig. 4.4h), no such decrease in spatial densitiy is visible. This is only possible if the detected summer events persist longer. A limited analysis of the duration of North American Z'_{300} cut-off lows indeed shows that detected events last on average 72 hours in winter, and 141 hours in summer, indicating an overestimation of cut-off low persistence during summer if TRACK is used with the current configuration. Further excluding weak feature points, or decreasing the upper-bound displacement d_{max} might result in more plausible results in terms of duration and seasonality, though further

---

[1]Any other season might be chosen for comparison. In this example winter was chosen, as it shows a weak pattern in terms of spatial density.

analysis on the tuning of the parameter is needed.

Both climatologies detect the least intense cut-off lows in summer, which is consistent with Southern Hemisphere 300 hPa cut-off lows (Pinheiro et al. (2019)), but not with Southern Hemisphere 500 hPa cut-off lows (Fuenzalida et al. (2005)), where no seasonality in cut-off low intensity was found. None of the previously mentioned studies on Northern Hemisphere cut-off lows consider cut-off low intensity, so no comparisons can be made. Yet, the intensity distributions for both the ξ_{300} as well as the Z'_{300} climatology echo the seasonal variation in jetstream intensity, namely a weaker (stronger) jetstream in summer (winter) due to the seasonal variation in the meridional temperature gradient between the equator and the pole.

5. Conclusion and Future Work

The cyclone detection tool TRACK is a potential alternative to pre-existing cut-off low detection schemes, though further analysis for the sensitivity of the algorithm to the configuration have to be performed. For example, setting the threshold for the feature point detection to a higher value excludes weaker systems. It is not clear yet how sensitive the approach and the derived characteristics of cut-off lows in the Northern Hemisphere are to this threshold, and the exclusion of very weak systems might improve the results significantly. For instance, the current configuration overestimates the persistence of summer cut-off lows over the North American domain, which is the season where the weakest systems are being detected. Increasing the feature point threshold might lead to a more realistic duration of cut-off lows in summer. Furthermore, sensitivity testing should also be applied to the adaptive constraints, as very restrictive constraints can lead to the separation of tracks, increasing the number of events and decreasing their persistence (and vice versa). In the future, results should be verified by visual inspection of e.g. geopotential height maps, to quantify the rate of failure when using TRACK.

Similar to what has been documented for the Southern Hemisphere (Pinheiro et al. (2020)), the choice of cut-off low detection method seems to be one of the main sources of uncertainty in the Northern Hemisphere as well. Assuming a cold cut-off low center at very high pressure levels misses cut-off lows in certain regions (Guo et al. (2021)), while the detection scheme used in the present work most likely overestimates cut-off low occurrence in general. For now, the best choice of detection method depends on the use case, and if preference is given to detecting as many events as possibly or detecting a limited amount of events all inhabiting a certain structure. The most robust statements on cut-off lows can be made on those aspects where both detection schemes agree, which are the low number of cut-off low occurrence in winter, their relatively short duration and some favoured regions of occurrences such as North America, Europe and Eastern Asia. Confidence in detection schemes could be improved by an intercomparison project similar to the Intercomparison of Mid Latitude Storm Diagnostics (IMILAST) experiment on the detection and tracking of extratropical cyclones (Neu et al. (2003)), in order to remove uncertainties regarding the usage of different datasets, observation periods and the subjective choice of parameters.

The detection and tracking on a relative vorticity field yields different results compared to the geopotential field in terms of number, region of occurrence and seasonality. Similar to what has been documented in Pinheiro et al. (2019), detection on a relative vorticity field results in more events being detected at lower latitudes, where the geopotential gradient is usually weak.

Even after the pre-processing steps, which aim to reduce the latitudinal influence in the geopotential height field, a weaker cut-off low density has been detected at lower latituded for the Z'_{300} climatology. The intensities derived from both fields show a similar distribution, indicating that the choice of field does not affect the type of system detected. Which field might be more suitable to detect cut-off lows is hard to say, as both fields focus on different spatial scales (Hoskins and Hodges (2002)). Future work might also examine the events detected on both fields separately from those detected in only one of them, to further strengthen the understanding on how the choice of field affects cut-off low detection.

While the current work gives a new perspective on Northern Hemisphere cut-off lows, further impact-based analysis is necessary to address the needs of stakeholders and policy makers, especially in terms of associated extreme precipitation. To this day there is no research of the vertical structure of cut-off lows for the entire Northern Hemisphere, and limited research has been performed on the prerequisites and impacts of cut-off low associated extreme precipitation events. A deeper knowledge on these topics can help to refine existing methods, and improve the assessment of their credibility. In the future, detection schemes might also include the position of the jetstream to ensure the poleward origin of the cut-off low, or make use of pattern recognition algorithms used in machine learning. Also, it is not clear how sensitive the detection tools are to anthropogenic climate change, and if certain methods might detect an artificial trend, e.g. by a change in location and magnitude of the cold core due to changes in the thermodynamic

components of the atmosphere, or a change in pressure gradient. While the current work highlights the sensitivity of the detection of Northern Hemisphere cut-off lows to the scheme used, it is indispensable to further analyse what kind of systems were detected (in terms of the associated impact), how high the rate of false positives is when using TRACK with the current configuration (by the visual inspection of e.g. geopotential height maps), apply different configurations to the algorithm, and determine if certain detection schemes differ in their skill of detecting extreme events.

Appendix

Appendix A.

TRACK - Adaptive Constraints

The following equations describe the feature tracking with adaptive constraints, adapted from Hodges (1999). The cost function Ξ is given as

$$\Xi = \sum_{i=1}^{m} \sum_{k=2}^{n-1} \mathscr{D}(P_i^{k-1}, P_i^k, P_i^{k+1}), \tag{A.1}$$

with the local deviation $\mathscr{D}$ at time step k for track i, where m is being the total number of tracks and n the total number of time steps. The local deviation is a function of the position vector P_i^k in three consecutive frames,

and is defined as

$$\mathscr{D}(P_i^{k-1}, P_i^k, P_i^{k+1}) = \begin{cases} 0, & \text{if } P_i^{k-1} \text{ is a phantom feature} \\ & \text{point, and } P_i^k \text{ and } P_i^{k+1} \text{ are} \\ & \text{real or phantom.} \\ \psi(P_i^{k-1}, P_i^k, P_i^{k+1}), & \text{if } P_i^{k-1}, P_i^k, \text{ and } P_i^{k+1} \text{ are real} \\ & \text{feature points.} \\ \Psi, & \text{otherwise.} \end{cases}$$

$$(A.2)$$

Phantom feature points are a computational convenience, first introduced by Salari and Sethi (1990). They do not carry any information and are used to pad out incomplete tracks, which is necessary to account for the appearance and disappearance of features. For real feature points in three consecutive frames, the local deviation $\mathscr{D}$ is defined as the local track smoothness function ψ, which is given by

$$\psi(P_i^{k-1}, P_i^k, P_i^{k+1}) = 0.5 \, w_1 \left(1 - \hat{T}_i^{(k-1,k)} \cdot \hat{T}_i^{(k,k+1)} \right)$$

$$+ w_2 \left(1 - \frac{2 \left[\left\| P_i^{k-1} P_i^k \right\| \, \left\| P_i^k P_i^{k+1} \right\| \right]^{1/2}}{\left[\left\| P_i^{k-1} P_i^k \right\| + \left\| P_i^k P_i^{k+1} \right\| \right]} \right). \qquad (A.3)$$

The first term is a measure of directional similarity and the second term a measure of speed similarity, scaled by the weights w_1 and w_2. The weights are set by the user, and specify the contribution of changes in direction, as well as changes in speed to the overall track smoothness. Slow-moving systems, for example, are expected to experience greater changes in direction

and smaller changes in velocity, compared to fast-moving systems. For the results presented in section 4 the weights were set to $w_1 = 0.2$ and $w_2 = 0.8$ respectively.

The local track smoothness ψ is limited by an upper bound Ψ_{max}, which satisfies the condition

$$\Psi_{max} \geq \sup_{d_i^{(k-1,k)}, d_i^{(k,k+1)} \in [0,D]} \psi_{max}\left(d_i^{(k-1,k)}, d_i^{(k,k+1)}\right). \qquad \text{(A.4)}$$

The upper-bound track smoothness constraint $\psi_{max}\left(d_i^{(k-1,k)}, d_i^{(k,k+1)}\right)$ is a function of the mean displacement over three consecutive frames, with $d_i^{(k-1,k)} = \left\|P_i^{k-1}P_i^k\right\|$ being either the geodesic norm for a spherical domain, or the euclidean norm for a cartesian domain. If P_i^{k-1} and/or P_i^k are phantom points, the norm is replaced by the global upper bound displacement D, defined as

$$D = \max_{\{j=1,N\}}\left(d_{max}^{(j)}\right), \qquad \text{(A.5)}$$

for $N =$ number of regions, and $d_{max}^{(j)}$ being the upper-bound displacement for region j.

Bibliography

Abatzoglou, J. T. (2016). Contribution of cutoff lows to precipitation across the united states*. *J. Appl. Meteor. Climatol.*, *55*(4), 893–899. https://doi.org/10.1175/JAMC-D-15-0255.1

Awan, N. K., & Formayer, H. (2017). Cutoff low systems and their relevance to large-scale extreme precipitation in the european alps. *Theor Appl Climatol*, *129*, 149–158. https://doi.org/10.1007/s00704-016-1767-0

Bell, G. D., & Bosart, L. F. (1989). A 15-year climatology of northern hemisphere 500 mb closed cyclone and anticyclone centers. *Mon. Wea. Rev*, *117*(10), 2142–2164. https://doi.org/10.1175/1520-0493(1989)117⟨2142:AYCONH⟩2.0.CO;2

Bozkurt, D., Rondanelli, R., Garreaud, R., & Arriagada, A. (2016). Impact of warmer eastern tropical pacific sst on the march 2015 atacama floods. *Mon. Wea. Rev.*, *144*(11), 4441–4460. https://doi.org/10.1175/MWR-D-16-0041.1

Crocker, A. M., Godson, W. L., & Penner, C. M. (1947). Frontal contour charts. *J. Meteor.*, *4*(3), 95–99. https://doi.org/10.1175/1520-0469(1947)004⟨0095:FCCBPO⟩2.0.CO;2

Delgado, G., Redaño, A., Lorente, J., Nieto, R., Gimeno, L., Ribera, P., Barriopedro, D., García-Herrera, R., & Serrano, A. (2007). Cloud cover analysis associated to cut-off low-pressure systems over europe using meteosat imagery. *Meteorol. Atmos. Phys.*, *96*, 141–157. https://doi.org/10.1007/s00703-006-0225-4

Dierckx, P. (1981). An algorithm for surface fitting with spline functions. *IMA J. Numer. Anal.*, *1*(3), 267–283. https://doi.org/10.1093/imanum/1.3.267

Dierckx, P. (1984). *Algorithms for smoothing data on the sphere with tensor product splines.* https://doi.org/10.1007/BF02243776

Emanuel, K. (2005). Genesis and maintenance of mediterranean hurricanes. *Adv. Geosci.*, *2*, 217–220. https://doi.org/10.5194/adgeo-2-217-2005

Fuenzalida, H. A., Sánchez, R., & Garreaud, R. D. (2005). A climatology of cutoff lows in the southern hemisphere. *J. Geophys. Res.*, *110*(D18101). https://doi.org/10.1029/2005JD005934

Goldfarb, D. (1969). Extension of davidons variable metric method to maximization under linear inequality and equality constraints. *SIAM J. Appl. Math.*, *17*(4), 739–764. https://doi.org/10.1137/0117067

Guo, N., Zhuo, Y., & Yang, L. (2021). Statistical analysis of central asian vortices and their influence on precipitation in xinjiang. *Atmospheric Research*, *249*, 105327. https://doi.org/10.1016/j.atmosres.2020.105327

Hersbach, H., Bell, B., Berrisford, P., Hirahara, S., Horányi, A., Muñoz-Sabater, J., Nicolas, J., Peubey, C., Radu, R., Schepers, D., Simmons, A., Soci, C., Abdalla, S., Abellan, X., Balsamo, G., Bechtold, P., Biavati, G., Bidlot, J., Bonavita, M., . . . Thépaut, J. (2020). The era5 global

reanalysis. *Q J R Meteorol Soc.*, *146*, 1999–2049. https://doi.org/10.1002/qj.3803

Hodges, K. I. (1994). A general method for tracking analysis and its application to meteorological data. *Mon. Wea. Rev.*, *122*(11), 2573–2586. https://doi.org/10.1175/1520-0493(1994)122⟨2573:AGMFTA⟩2.0.CO;2

Hodges, K. I. (1995). Feature tracking on the unit sphere. *Mon. Wea. Rev*, *123*(12), 3458–3465. https://doi.org/10.1175/1520-0493(1995)123⟨3458:FTOTUS⟩2.0.CO;2

Hodges, K. I. (1999). Adaptive constraints for feature tracking. *Mon. Wea. Rev.*, *127*(6), 1362–1373. https://doi.org/10.1175/1520-0493(1999)127⟨1362:ACFFT⟩2.0.CO;2

Hoskins, B. J., & Hodges, K. I. (2002). New perspectives on the northern hemisphere winter storm tracks. *J. Atmos. Sci.*, *59*(6), 1041–1061. https://doi.org/10.1175/1520-0469(2002)059⟨1041:NPOTNH⟩2.0.CO;2

Hoskins, B. J., McIntyre, M. E., & Robertson, A. W. (1985). On the use and significance of isentropic potential vorticity maps. *Q.J.R. Meteorol. Soc.*, *111*, 877–946. https://doi.org/10.1002/qj.49711147002

Hsieh, Y. P. (1949). An investigation of a selected cold vortex over north america. *J. Meteor.*, *6*(6), 401–410. https://doi.org/0.1175/1520-0469(1949)006⟨0401:AIOASC⟩2.0.CO;2

Kentarchos, A. S., & Davies, T. D. (1998). A climatology of cut-off lows at 200 hpa in the northern hemisphere, 1990–1994. *Int. J. Climatol*, *18*, 379–390. https://doi.org/10.1002/(SICI)1097-0088(19980330)18:4⟨379::AID-JOC257⟩3.0.CO;2-F

Llasat, M. C., Martín, F., & Barrera, A. (2007). From the concept of "kaltluft-tropfen"(cold air pool) to the cut-off low. the case of september 1971 in spain as an example of their role in heavy rainfalls. *Meteorol Atmos Phys*, *96*, 43–60. https://doi.org/10.1007/s00703-006-0220-9

Manganello, J. V., Hodges, K. I., Dirmeyer, B., III, J. L. K., Cash, B. A., Marx, L., Jung, T., Achuthavarier, D., Adams, J. M., Altshuler, E. L., Huang, B., Jin, E. K., Towers, P., & Wedi, N. (2014). Future changes in the western north pacific tropical cyclone activity projected by a multidecadal simulation with a 16-km global atmospheric gcm. *J. Climate*, *27*(20), 7622–7646. https://doi.org/10.1175/JCLI-D-13-00678.1

Muñoz, C., Schultz, D., & Vaughan, G. (2020). A midlatitude climatology and interannual variability of 200- and 500-hpa cut-off lows. *J. Climate*, *33*(6), 2201–2222. https://doi.org/10.1175/JCLI-D-19-0497.1

Ndarana, T., & Waugh, D. W. (2010). The link between cut-off lows and rossby wave breaking in the southern hemisphere. *Q.J.R. Meteorol. Soc.*, *136*, 869–885. https://doi.org/10.1002/qj.627

Neu, U., Akperov, M., Bellenbaum, N., Benestad, R., Blender, R., Caballero, R., Cocozza, A., Dacre, H., Fend, Y., Fraedrich, K., Grieger, J., Gulev, S., Hanley, J., Hewson, T., Inatsu, M., Keay, K., Kew, S., Kindem, I., Leckebusch, G., . . . Wernli, H. (2003). Imilast: A community effort to intercompare exratropical cyclone detection and tracking algorithms. *Bull. Amer. Meteor. Soc.*, *94*(4), 529–547. https://doi.org/10.1175/BAMS-D-11-00154.1

Nieto, R., Gimeno, L., de la Torre, L., Ribera, P., Gallego, D., García-Herrera, R., García, J. A., Nuñez, M., Redaño, A., & Lorente, J. (2005). Climatological features of cutoff low systems in the northern hemisphere. *J. Climate*, *18*(16), 3085–3103. https://doi.org/10.1175/JCLI3386.1

Nieto, R., Gimeno, L., la Torre, L. D., Ribera, P., Barriopedro, D., García-Herrera, R., Serrano, A., Gordillo, A., Redaño, A., & Lorente, J. (2007). Interannual variability of cut-off low systems over the european sector: The role of blocking and the northern hemisphere circulation modes. *Meteorol. Atmos. Phys.*, *96*, 85–101. https://doi.org/10.1007/s00703-006-0222-7

Nieto, R., Sprenger, M., Wernli, H., Trigo, R. M., & Gimeno, L. (2008). Identification and climatology of cut-off lows near the tropopause. *Ann. N.Y. Acad. Sci.*, *1146*, 256–290. https://doi.org/10.1196/annals.1446.016

Palmén, E. (1949). Origin and structure of high-level cyclones south of the: Maximum westerlies. *Tellus*, *1*, 22–31. https://doi.org/10.1111/j.2153-3490.1949.tb01925.x

Palmén, E., & Newton, C. W. (1969). *Atmospheric circulation systems: Their structure and physical interpretation* (J. van Mieghem, Ed.). Academic Press, Inc.

Pinheiro, H. R., Gan, M. A., & Hodges, K. I. (2020). Structure and evolution of intense austral cut-off lows. *Q.J.R. Meteorol. Soc.*, *n/a*(n/a). https://doi.org/10.1002/qj.3900

Pinheiro, H. R., Hodges, K. I., & Gan, M. A. (2019). Sensitivity of identifying cut-off lows in the southern hemisphere using multiple criteria:

Implications for numbers, seasonality and intensity. *Clim Dyn*, *53*, 6699–6713. https://doi.org/10.1007/s00382-019-04984-x

Porcù, F., Carrassi, A., Medaglia, C. M., Prodi, F., & Mugnai, A. (2007). A study on cut-off low vertical structure and precipitation in the mediterranean region. *Meteorol Atmos Phys*, *96*, 121–140. https://doi.org/10.1007/s00703-006-0224-5

Price, J. D., & Vaughan, G. (1992). Statistical studies of cut-off-low systems. *Annales Geophysicae*, *10*, 96–102.

Price, J. D., & Vaughan, G. (1993). The potential for stratosphere-troposphere exchange in cut-off-low systems. *Q.J.R. Meteorol. Soc.*, *119*, 343–365. https://doi.org/10.1002/qj.49711951007

Ravetta, F., & Ancellet, G. (2000). Identification of dynamical processes at the tropopause during the decay of a cutoff low using high-resolution airborne lidar ozone measurements. *Mon. Wea. Rev.*, *128*(9), 3252–3267. https://doi.org/10.1175/1520-0493(2000)128⟨3252:IODPAT⟩2.0.CO;2

Reboita, M. S., Nieto, R., Gimeno, L., da Rocha, R. P., Ambrizzi, T., Garreaud, R., & Krüger, L. F. (2010). Climatological features of cutoff low systems in the southern hemisphere. *J. Geophys. Res.*, *115*(D17104). https://doi.org/10.1029/2009JD013251

Salari, V., & Sethi, I. K. (1990). Feature point correspondence in the presence of occlusion. *IEEE Transactions on Pattern Analysis and Machine Intelligence*, *12*(1), 87–91. https://doi.org/10.1109/34.41387

Satyamurty, P., & Seluchi, M. E. (2007). Characteristics and structure of an upper air cold vortex in the subtropics of south america. *Meteorol. Atmos. Phys.*, *96*, 203–220. https://doi.org/10.1007/s00703-006-0207-6

Shepherd, M., Mote, T., Dowd, J., Roden, M., Knox, P., McCutcheon, S. C., & Nelson, S. E. (2011). An overview of synoptic and mesoscale factors contributing to the disastrous atlanta flood of 2009. *Bull. Amer. Meteor. Soc.*, *92*(7), 861–870. https://doi.org/10.1175/2010BAMS3003.1

Singleton, A. T., & Reason, C. J. C. (2007). A numerical model study of an intense cutoff low pressure system over south africa. *Mon. Wea. Rev*, *135*, 1128–1150. https://doi.org/10.1175/MWR3311.1

Thorpe, A. J., Volkert, H., & Heimann, D. (1993). Potential vorticity of flow along the alps. *J. Atmos. Sci.*, *50*(11), 1573–1590. https://doi.org/10.1175/1520-0469(1993)050⟨1573:PVOFAT⟩2.0.CO;2

Vessey, A. F., Hodges, K. I., Shaffrey, L. C., & Day, J. J. (2020). An intercomparison of arctic synoptic scale storms between four global reanalysis datasets. *Clim Dyn*, *54*, 2777–2795. https://doi.org/10.1007/s00382-020-05142-4

Wernli, H., & Sprenger, M. (2007). Identification and era-15 climatology of potential vorticity streamers and cutoffs near the extratropical tropopause. *J. Atmos. Sci.*, *64*, 1569–1586. https://doi.org/10.1175/JAS3912.1

Zappa, G., Hawcroft, M. K., Shaffrey, L., Black, E., & Brayshaw, D. J. (2015). Extratropical cyclones and the projected decline of winter mediterranean precipitation in the cmip5 models. *Clim Dyn*, *45*, 1727–1738. https://doi.org/10.1007/s00382-014-2426-8

Zhao, S., & Sun, J. (2007). Study on cut-off low-pressure systems with floods over northeast asia. *Meterol. Atmos. Phys.*, *96*, 159–180. https://doi.org/10.1007/s00703-006-0226-3